

Accelerated Articles*Anal. Chem.* 1994, 66, 2425–2432

Imaging with Ion Beams and Laser Postionization

M. Wood, Y. Zhou, C. L. Brummel, and N. Winograd**Department of Chemistry, The Pennsylvania State University, 152 Davey Laboratory, University Park, Pennsylvania 16802*

We investigate the use of a liquid metal ion gun (LMIG) combined with multiphoton resonance ionization of sputtered atoms and/or molecules to acquire mass-selected images with submicrometer spatial resolution. Images from several model systems are presented including those of an In grid, and of patterned surfaces of benzo[a]pyrene and tryptophan thin films. Since postionization for these systems yields ionization efficiencies that are considerably higher than those achieved with secondary ion mass spectrometry (SIMS), spatial resolution of 2600 Å for molecular species could be achieved while static conditions were maintained. Cooling of the sample to <210 K was shown to be essential for molecular systems since the number of thermally evaporating molecules overwhelms the number of sputtered molecules at room temperature. Other details necessary to incorporate laser postionization into a time-of-flight SIMS instrument using a pulsed LMIG source are also discussed.

New possibilities for chemical-specific imaging of surfaces have recently become possible by employing focused ion beams to desorb atoms and molecules from a small area using a liquid metal ion gun (LMIG).¹ For example, it is feasible to focus the incident ion beam to a spot size of less than 50 nm and with a flux density of better than 5 A/cm². If the resulting desorbed species are detected by mass spectrometry, and the incident ion beam is rastered across the target, it is possible to obtain mass-selected images with very high spatial resolution.^{2–6}

- (1) Orloff, J. *Rev. Sci. Instrum.* 1993, 64, 1105–1130.
- (2) Levi-Setti, R.; Hallegot, P.; Girod, C.; Chabala, J. M.; Li, J.; Sadonis, A.; Wolbach, W. *Surf. Sci.* 1991, 246, 94–100.
- (3) Chabala, J. M.; Levi-Setti, R.; Soni, K. K.; Williams, D. B.; Newbury, D. E. *Appl. Surf. Sci.* 1991, 51(3–4), 185–192.
- (4) Lampert, J. K.; Koerner, G. S.; Macaoay, J. M.; Chabala, J. M.; Levi-Setti, R. *Appl. Surf. Sci.* 1992, 55(2–3), 149–158.
- (5) Benninghoven, A.; Hagenhoff, B.; Niehuis, E. *Anal. Chem.* 1993, 65, 630A–640A.
- (6) Winograd, N. *Anal. Chem.* 1993, 65, 622A–629A.

Early experiments using a Ga LMIG were first reported by Levi-Setti and co-workers, who obtained chemical maps for elemental species using a quadrupole mass analyzer as the detector.^{7,8} Later, with the advent of time-of-flight (TOF) detection, the sensitivity was improved by many orders of magnitude because of the efficient transmission of ions through the TOF.^{9,10} Moreover, ions are counted in a parallel fashion, rather than by scanning a mass window, as is the case with either quadrupoles or magnetic sector machines. This improved efficiency allows images to be recorded in the “static” regime where damage from the incident beam is minimized. These instrumental advances have inspired several attempts to image molecular species that are desorbed by use of an LMIG with TOF detection,¹¹ with moderate success. As has been pointed out on numerous occasions, the analysis of submicrometer areas is limited by the availability of sample, generally on the order of only 10⁶ molecules/μm².^{2,6,11,12}

Since there is a fundamental issue of sensitivity associated with imaging by ion beams, a number of groups have investigated the possibility of enhancing the detection efficiency by employing methods to ionize the neutral atoms after they have desorbed from the surface.^{13–17} This approach, in principle at least, separates the desorption step from the ionization step and should also minimize some of the known matrix ionization effects that have plagued secondary ion mass

- (7) Levi-Setti, R.; Fox, T. R. *Nucl. Instrum. Methods* 1980, 168, 139–149.
- (8) Levi-Setti, R.; La Marche, P. H.; Lan, K.; Shields, T. H.; Wang, Y. L. *Nucl. Instrum. Methods Phys. Res.* 1983, 218, 368–374.
- (9) Chait, B. T.; Standing, K. G. *Int. J. Mass Spectrom. Ion Phys.* 1981, 40, 185–193.
- (10) Steffens, P.; Niehuis, E.; Friese, T.; Greifendorf, D.; Benninghoven, A. *J. Vac. Sci. Technol.* 1985, A3, 1322–1325.
- (11) Briggs, D.; Hearn, M. J. *Surf. Interface Anal.* 1988, 13, 181–185.
- (12) Gillen, G.; Simons, D. S.; Williams, P. *Anal. Chem.* 1990, 62, 2122–2130.
- (13) Winograd, N.; Baxter, J. P.; Kimock, F. M. *Chem. Phys. Lett.* 1982, 88, 581–584.
- (14) Parks, J. E.; Schmitt, H. W.; Hurst, G. S.; Fairbank, W. M. *Thin Solid Films* 1983, 108, 69–78.
- (15) Pellin, M. J.; Young, C. E.; Calaway, W. F.; Gruen, D. M. *Surf. Sci.* 1984, 144, 619–637.
- (16) Becker, C. H.; Gillen, K. T. *Appl. Phys. Lett.* 1984, 45, 1063–1066.
- (17) Terhorst, M.; Kampwerth, G.; Niehuis, E.; Benninghoven, A. *J. Vac. Sci. Technol. A* 1992, 10, 3210–3215.

spectrometry (SIMS) from time to time. Several schemes have been reported using lasers to positionize atoms and molecules desorbed by employing an LMIG. These schemes have involved the use of 248-nm radiation to nonselectively ionize the desorbed flux,¹⁸ multiphoton nonresonant ionization using subpicosecond pulses to minimize molecular photodissociation,¹⁹ and resonance-enhanced multiphoton ionization to maximize the sensitivity for a selected set of desorbed species.²⁰ Only a limited number of systems have been investigated so far using laser postionization, but the initial results indicate that it will be a valuable compliment to imaging SIMS with submicrometer spatial resolution.

In this work, we investigate a number of the issues that need to be considered when attempting to utilize laser postionization with an LMIG source. These include the development of special extraction optics to maximize the detection efficiency and mass resolution for both SIMS and laser postionization experiments, and the use of a cryogenic stage to minimize the presence of background signal due to the finite vapor pressure of most molecular species. Moreover, we show that the efficiency of detection of atomic species now approaches the theoretical limit, but that the efficiency of ionization of molecular species is generally still not adequate.

EXPERIMENTAL SECTION

The instrumentation employed in this work is a modified version of a PRISM imaging TOF-SIMS manufactured by Kratos, Inc. We employ an LMIG from FEI Inc. as the microprobe source and a 4.5-m reflecting mirror analyzer as the TOF analyzer. The analyzer has a nominal mass resolution in excess of 1 part in 10 000 Da, as determined using the full width at half-maximum of the peak, with transmission of ~50%. Laser postionization is accomplished using a Spectra-Physics GCR 5–30 Hz YAG laser to pump a PDL-3 dye laser and a WEX-1 frequency doubler. A schematic diagram is shown in Figure 1. Details of this apparatus have been published including a discussion of issues related to timing sequences, pulsing schemes, and ion detection strategies.^{13,21–24} Modifications relative to this work are presented below.

(a) Ion Source Details. The LMIG offers a unique source with spatial resolution approaching 200 Å. For the source employed in this work, there are two selectable apertures in the focusing column which yield beam sizes of 2000 or 500 Å. The current associated with the larger spot is 500 pA at 25 keV (1.6 A/cm²) while the smaller spot yields 60 pA (3 A/cm²). This ion beam current corresponds to 3.1 Ga⁺ ions/ns for the larger beam and 0.37 Ga⁺ ions/ns for the smaller beam. For example, for the 500-pA beam, there will be 78 000 Ga⁺ ions/s striking the target in a typical SIMS experiment which employs a 5-ns incident pulse and a repetition rate of 5 kHz. For the corresponding laser postionization experiment,

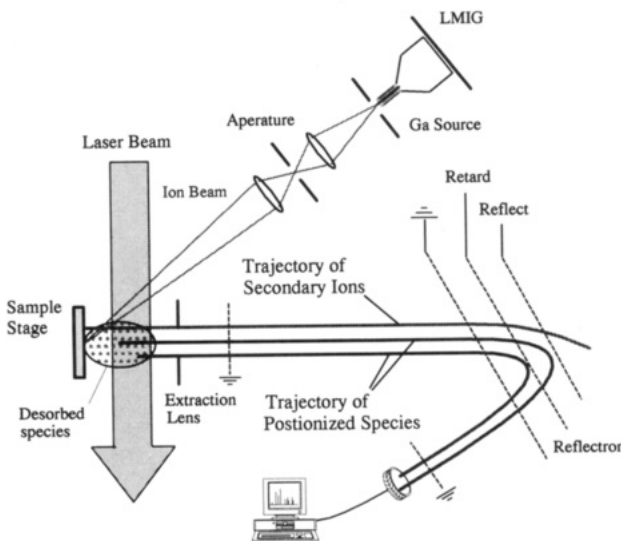


Figure 1. Schematic diagram of the TOF-SIMS imaging system with postionizing laser.

there would be 56 000 Ga⁺ ions/s striking the target, assuming a 600-ns incident Ga⁺ ion pulse repeated at 30 Hz.

When laser postionization is employed, the LMIG is pulsed to maximize the sampling efficiency. Choice of the optimal pulse duration presents a number of challenges and opportunities. For TOF-SIMS applications, the ion beam is directed through the aperture by a high-speed voltage applied to a set of blanking plates. For optimal mass resolution, beam pulses of ~2 ns in length can be achieved using this approach. Moving the beam in and out of the aperture, however, causes a small amount of motion of the ion beam on the sample, leading to a concomitant loss of spatial resolution. For laser postionization experiments, the optimal pulse length is at least 100 times longer than the optimal SIMS pulse width, i.e., a value of 200–1000 ns.¹³ This configuration reduces the influence of the movement of the beam on the surface and, in principle at least, allows TOF measurements to approach the same spatial resolution that is associated with the dc beam. Moreover, the longer pulse times at least partially compensate for the low repetition rate of the laser experiment (30 Hz) when compared to the SIMS experiment (5–10 kHz) by effectively increasing the duty cycle.

(b) Laser Postionization Extraction Optics. There are special criteria required to combine high performance imaging TOF-SIMS instrumentation with resonance-enhanced laser postionization. As shown schematically in Figure 2B, particles emitted from the surface should be collected and collimated with the appropriate combination of optics and potentials to maximize the extraction efficiency and to maximize mass resolution in a TOF environment. Resonance ionization experiments generally employ unfocused lasers since less power density is required and a larger effective ionization volume yields a better spatial overlap factor between the laser field and the sputtered plume of particles.^{21–24} Postionization is problematic for high performance extraction optics for this situation due to the large potential gradients which develop across the finite volume presented by the laser beam. For optimal SIMS imaging without postionization, for example, we employ an extraction potential of 7.2 keV between the sample and the front surface of the lens 4 mm above the sample.

- (18) Mouncey, S. P.; Moro, L.; Becker, C. H. *Appl. Surf. Sci.* **1991**, *52*, 39–44.
- (19) Terhorst, M.; Möllers, R.; Niehuis, E.; Benninghoven, A. *Surf. Interface Anal.* **1992**, *18*, 824–826.
- (20) Winograd, N.; Zhou, Y.; Wood, M. C.; Lakiszak, S. *RIS 92 Inst. Phys. Conf. Ser.* **1992**, *128*, 259–264.
- (21) Kimock, F. M.; Baxter, J. P.; Pappas, D. L.; Kobrin, P. H.; Winograd, N. *Anal. Chem.* **1984**, *56*, 2782–2791.
- (22) Pappas, D. L.; Hrubowchak, D. M.; Ervin, M. H.; Winograd, N. *Science* **1989**, *243*, 64–66.
- (23) Hrubowchak, D. M.; Ervin, M. H.; Wood, M. C.; Winograd, N. *Anal. Chem.* **1991**, *63*, 225–232.
- (24) Ervin, M. H.; Wood, M. C.; Winograd, N. *Anal. Chem.* **1993**, *65*, 417–420.

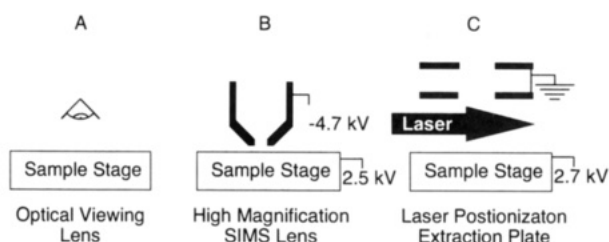


Figure 2. Schematic diagram depicting the three available modes of sample viewing: (A) the optical viewing scheme, (B) the extraction optics for SIMS, and (C) the arrangement for efficient extraction of positionized neutral species. Note that the sample stage is biased to +2.5 keV for SIMS analysis and to +2.7 keV for laser postionization experiments. The voltages are set for positive ion detection in all cases.

A laser beam that is 1 mm in diameter would produce ions with an energy dispersion of $(1/4)(7200 \text{ eV}) = 1800 \text{ eV}$, a value too large to be compensated by the TOF analyzer.

To alleviate this difficulty, three different lenses are mounted on a revolving carousel holder which allows the viewing mode to be modified in vacuum, as shown schematically in Figure 2. One position is occupied by an optical microscope objective for sample positioning, a second position is occupied by the high-field SIMS extraction lens, and the third position is occupied by a second extraction system optimized for laser postionization. The lenses can each be rotated into position in vacuum. The laser postionization lens consists simply of two grounded plates with a central aperture for transmission of ions. The lens is positioned ~1 cm from the sample and can extract ions from a laser beam which is ~1.5 mm in diameter. The extraction volume was determined by optimizing the count rate for photoionized species while changing the diameter of the laser beam. The potential between the extraction lens and stage is increased to ~2.7 kV to compensate for the energy deficiency these ions experience by being created within the gap. The energy dispersion of the photoions is 270 V for a 1-mm laser beam, a value easily compensated by the TOF analyzer.

(c) Laser Postionization Wavelengths. We have investigated the feasibility of achieving submicrometer imaging by resonant ionization of atomic and/or molecular species. Atomic species, in general, yield bigger signals than molecules and provide a good reference point to evaluate system performance. Indium has been chosen as a test system as it ionizes efficiently at easily attainable laser wavelengths.²¹ The MPRI scheme employs a 303.9-nm pulse to pump the $^2\text{D}_{3/2}$ state and a 607.9-nm photon for ionization. The laser energies employed in this experiment were 0.86 and 7.0 mJ/pulse constricted to ~1.5 mm for 304 and 608 nm, respectively. For molecular systems, the gas-phase absorbance spectra were employed to obtain the resonance wavelength. For systems containing an aromatic ring, 280-nm light was employed for ionization.^{23,24} One photon of 280 nm is used to pump the π to π^* transition, and a second photon of 280 nm is employed for ionization. The laser energies employed for postionization of benzo[a]pyrene and tryptophan were typically 1–5 mJ/pulse to optimize intensity of the molecular ion and minimize fragmentation.

(d) Sample Cryogenic Stage. To reduce the background signal from target molecules with a finite vapor pressure, it

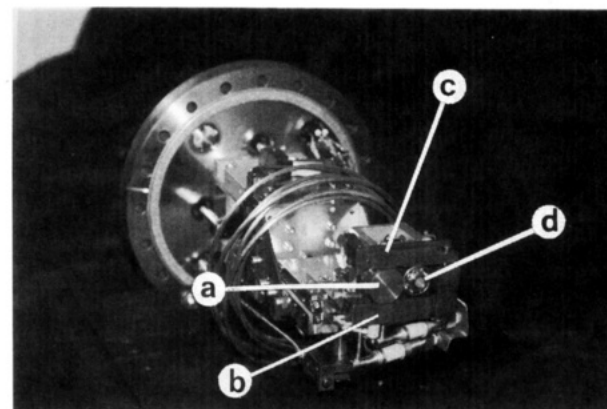
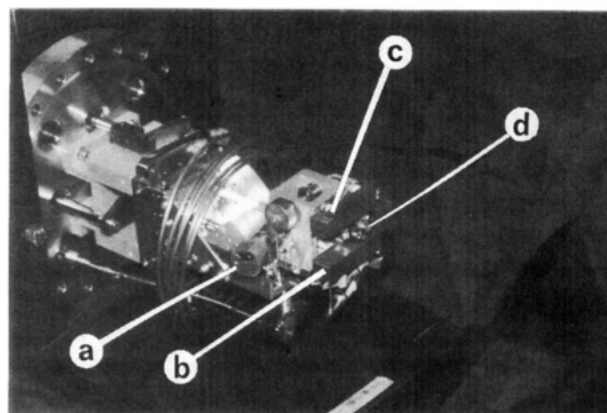


Figure 3. Photographs of the cryogenic stage and manipulator with sample holder. See text for details of operation.

is desirable to be able to cool the sample to temperatures approaching 77 K. Issues related to sample cooling have been discussed in detail previously, where it was shown that a variety of samples, including frozen solutions, are amenable to characterization using the MPRI approach.²⁴ For the experiments described in this work, the requirements are even more stringent because of the low incident beam current associated with the LMIG source. For example, a 60-pA Ga^+ ion pulsed for 100 ns may yield less than $\sim 10^2$ sputtered species, corresponding to an instantaneous pressure of $\sim 10^{-11}$ Torr. In our earlier work,²⁴ the unfocused duoplasmatron primary ion gun produced a current of $\sim 1 \mu\text{A}$ which desorbs $\sim 10^{-7}$ Torr of sputtered species.

The design of the cold stage for these experiments is shown in Figure 3. The front view of a removable copper sample stub (part a) is clamped to a liquid nitrogen reservoir (part b) by a metal bar (part c). This sample stub is locked on a copper holder which is connected to a rotatable Torlon rod. The sample is cooled by flowing liquid nitrogen through the reservoir during the experiments. Both the sample and liquid nitrogen reservoir are electrically isolated from the ground since the sample is held at 2.5 kV under operating conditions. This reservoir reaches the base temperature of 80 K in 10 min. The liquid nitrogen flow rate can be adjusted to change the cooling speed. During the sample transfer, the copper claw bar (part c) is opened by rotating the nonconcentric ring (part d). The sample stub is then moved out of the cooling region by rotating the Torlon rod connected to the copper holder. The sample reaches the temperature of the reservoir within a few seconds after thermal contact is achieved. The

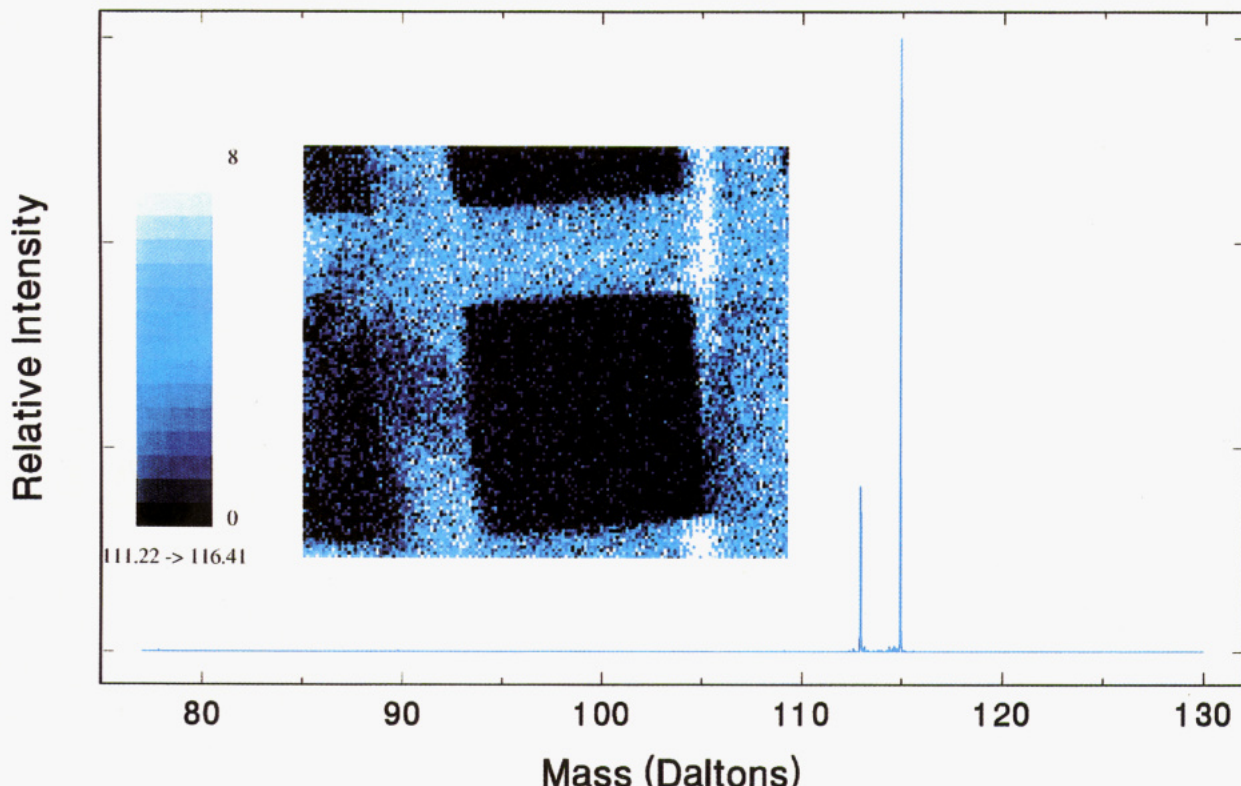


Figure 4. TOF spectrum of In atoms desorbed from an indium-coated Cu grid by 25-keV Ga^+ ions. The In atoms are resonantly ionized using the laser scheme described in the text. The signal was obtained from the sum of 3000 ion pulses of 300-ns duration, or 337 500 Ga^+ ions. Note that the isotope ratio deviates from the predicted value of 4% due to saturation of the ^{115}In signal. The In image of this grid is shown in the inset. The image size is $100\text{ }\mu\text{m} \times 84\text{ }\mu\text{m}$. Each pixel measures 6600 \AA on each side. The image was acquired with a total dose of $3 \times 10^9\text{ Ga}^+/\text{cm}^2$. The mass resolution of the In spectrum is ~ 3000 .

sample transfer arm is also cooled with a liquid nitrogen jacket. Typically, moving the sample from the transfer rod to the cooling stage takes ~ 1 min.

RESULTS AND DISCUSSION

The goal of this work is to examine the feasibility of utilizing MPRI positionization combined with high-performance TOF-SIMS instrumentation for chemical mapping with submicrometer spatial resolution. In this section, we first present results obtained using In as a model system since it yields the largest signals we are likely to see for a given experimental setup. With performance characteristics obtained using In, we then examine the possibility of characterizing patterned molecular surfaces. The results provide new insight into possible experimental complexities and suggest new directions for overcoming a number of these difficulties.

(a) Atomic Imaging Using Indium. The approach to chemical mapping is illustrated in Figure 4 by the image of an In-coated grid and its corresponding TOF spectrum. The initial issue involves the mechanism by which the photoions are counted. In general, TOF-SIMS spectra are recorded using a single-stop time-to-digital (TDC) converter with registration times which vary from 156 ps to several nanoseconds. For laser positionization experiments, several hundred atomic ions may be produced after each laser shot, each arriving at the microchannel plate detector at approximately the same time. Hence, neither single-stop nor the newer multistop TDCs are well-suited detectors for these experiments. Transient digitizers circumvent these problems by simply

digitizing the output current from the channel plate as a function of time. Time resolution to 500 ps is currently feasible. For imaging applications, however, data transfer between the digitizer and the image processor computer is required after acquisition of the mass spectrum associated with a individual pixel. This transfer time is often much slower than the laser pulse repetition rate. At this time, there is no ideal solution to this problem, and compromises must be made.

In our experiments, two different procedures have been followed. If ultimate mass resolution is required, the incident beam current is attenuated such that less than one count per laser pulse reaches the detector. A single-stop TDC may then be employed to record the spectrum with the desired time resolution. This procedure also facilitates the quantitation of ion yields since there is no ambiguity about what constitutes the presence or absence of a single ion. If higher count rates are required, we employ a multihit TDC with 10-ns time registration and a 2-ns dead time. With this scheme, up to three counts per mass peak may be recorded without introducing distortions. Higher count rates may also be obtained by intentionally detuning the TOF analyzer to broaden the arrival times of the ions.

From the spectrum shown in Figure 4, it is straightforward to calculate the useful yield of In atoms. Using the multihit TDC, we find $1.3\text{ }^{113}\text{In}^+$ ions per laser shot, corresponding to $32\text{ }^{115}\text{In}^+$ ions per laser shot using a 300-ns, 60-pA Ga^+ ion incident beam pulse. The magnitude of the ion beam current is determined from the dc beam using a Faraday cup. Assuming a yield of nine In atoms per incident Ga^+ ion, there

are $(112 \text{ Ga} \times 9 \text{ In/Ga})$ or ~ 1000 In atoms generated per pulse, giving a useful yield of $33/1000 = 3.3\%$. The major uncertainty in this estimate is the yield of In atoms per incident Ga^+ ion. Previous estimates, based on a value of 3 In atoms/ Ga^+ ion, for example, give useful yield of 9%.^{6,20} Under ideal circumstances, we expect the analyzer to have $\sim 50\%$ transmission efficiency, and the extraction optics to draw $\sim 50\%$ of the ions into the analyzer. If we assume 100% ionization efficiency and a 50% overlap of the sputtered atoms with the laser beam, then the maximum possible useful yield is less than 12%. Hence, our observed values are within striking range of the theoretical limit.

Creating a chemical map from the spectrum shown in Figure 4 is straightforward. The counts of $^{113}\text{In}^+$ and $^{115}\text{In}^+$ are summed and recorded as a function of ion beam position as it is rastered over the surface. As shown in Figure 4, variations in concentration of In over the surface are easily seen. For the image shown, each pixel measures $6600 \text{ \AA} \times 6600 \text{ \AA}$ and the total field of view is $100 \mu\text{m} \times 84 \mu\text{m}$. Image acquisition time is generally quite long and is seriously limited by the pulse repetition rate of the laser. In this case, each pixel was recorded using two laser shots and there are $\sim 20\,000$ pixels (152×128) in the image, resulting in an acquisition time of 21 min. This image does not exhibit particularly high spatial resolution, although we have recently reported images with resolution near 1000 \AA .⁶ Of special interest, however, is that the primary ion dose necessary to obtain this picture was only $3 \times 10^9 \text{ Ga}^+ \text{ ions/cm}^2$. This value is well below the static limit of $10^{12}\text{--}10^{13} \text{ Ga}^+ \text{ ions/cm}^2$ and suggests that if similar ionization efficiencies are possible with molecules, molecular mapping may indeed be feasible with this approach.

(b) Molecule-Specific Imaging. Molecular photoionization and its use with various desorption techniques has been discussed for many years. Although this methodology offers a powerful complement to static SIMS experiments, there are two major issues which have remained problematic. First, to obtain the necessary molecular ionization efficiency, the laser power must be increased to the point where molecular fragmentation begins to dominate the mass spectrum. This issue has been addressed by using resonance-enhanced ionization schemes where cross sections are higher and by utilizing picosecond or subpicosecond pulses²⁵⁻²⁸ to achieve photoionization before fragmentation can occur. Both of these approaches are finding a degree of success. The second major issue involves the nonzero vapor pressure exhibited by virtually all molecular species at room temperature. We have reported this problem earlier²⁴ and have found a significant background due to thermally evaporating molecules as compared to the sputtered yield even when using an ion source with a current of $\sim 1 \mu\text{A}$. For experiments reported here, this process has catastrophic consequences since the LMIG current is 4 orders of magnitude smaller than this value, while the molecular evaporation rate remains the same.

To illustrate the scope of this problem, we utilize benzo[*a*]pyrene as a test case. The vapor pressure of this molecule

(25) Möllers, R.; Terhorst, M.; Niehuis, E.; Benninghoven, A. *Org. Mass Spectrom.* 1992, 27, 1393-1395.

(26) Hering, P.; Maaswinkel, A. G. M.; Kompa, K. L. *Chem. Phys. Lett.* 1981, 83, 222-225.

(27) Dyer, M. J.; Jusinski, L. E.; Helm, H.; Becker, C. H. *Appl. Surf. Sci.* 1991, 52, 151-157.

(28) Becker, C. H.; Hovis, J. S. *J. Vac. Sci. Technol.*, in press.

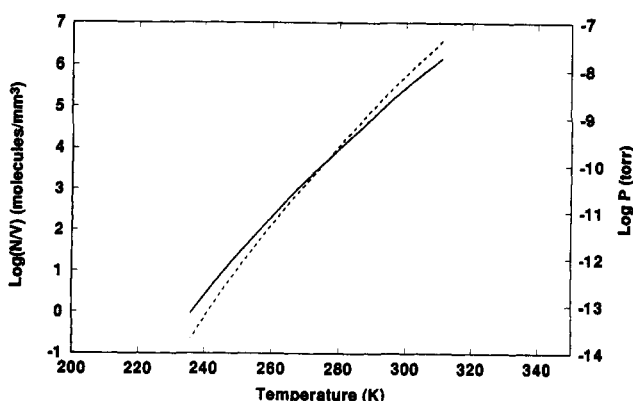


Figure 5. Plot of vapor pressure and the number of molecules per volume of benzo[*a*]pyrene as a function of temperature. The solid lines demonstrate the $\log(N/V)$ curve while the dotted line shows the $\log(\text{Torr})$ curve.

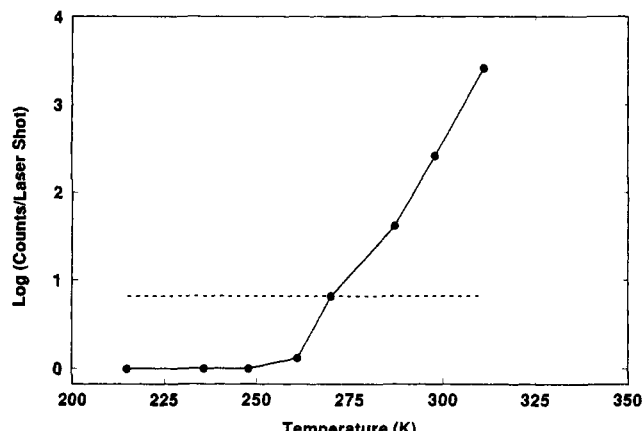


Figure 6. Plot of experimentally detected gas-phase benzo[*a*]pyrene molecules as a function of temperature. The dotted line indicates the approximate intensity of the molecular ion signal of sputtered benzo[*a*]pyrene.

has been measured as a function of temperature between 358 and 431 K and fit to the relation

$$\log P = -(A/T) + B \quad (1)$$

where P is the pressure in atmospheres and A and B are fitting parameters.²⁹ For this case, $A = 6181 \pm 32$ and $B = 9.60 \pm 0.083$. The number of molecules, N , in a 1-mm³ volume may then be computed from the ideal gas law. The expected value for $\log(N/V)$ (in this case, the number of molecules in a 1-mm³ volume) or pressure is plotted as a function of temperature in Figure 5. At 310 K, there are expected to be 1.3×10^6 molecules/mm³ above the surface of the benzo[*a*]pyrene sample.

These predictions may easily be checked by experiment, at least qualitatively. In Figure 6, we show the intensity of the benzo[*a*]pyrene molecular ion signal at m/z 252, recorded 0.5 mm above a thin film of benzo[*a*]pyrene, as a function of the target temperature. The gas-phase molecule was photoionized using 280-nm photons, and the intensity was obtained by averaging the results from 3000 laser pulses. At 310 K, we find 2730 molecular ions per pulse. The expected yield from sputtered molecules, as noted below, is in the range of 10 molecular ions per pulse. The gas-phase signal is strongly

(29) Murray, J. J.; Pottie, R. F.; Pupp, C. *Can. J. Chem.* 1974, 52, 557-563.

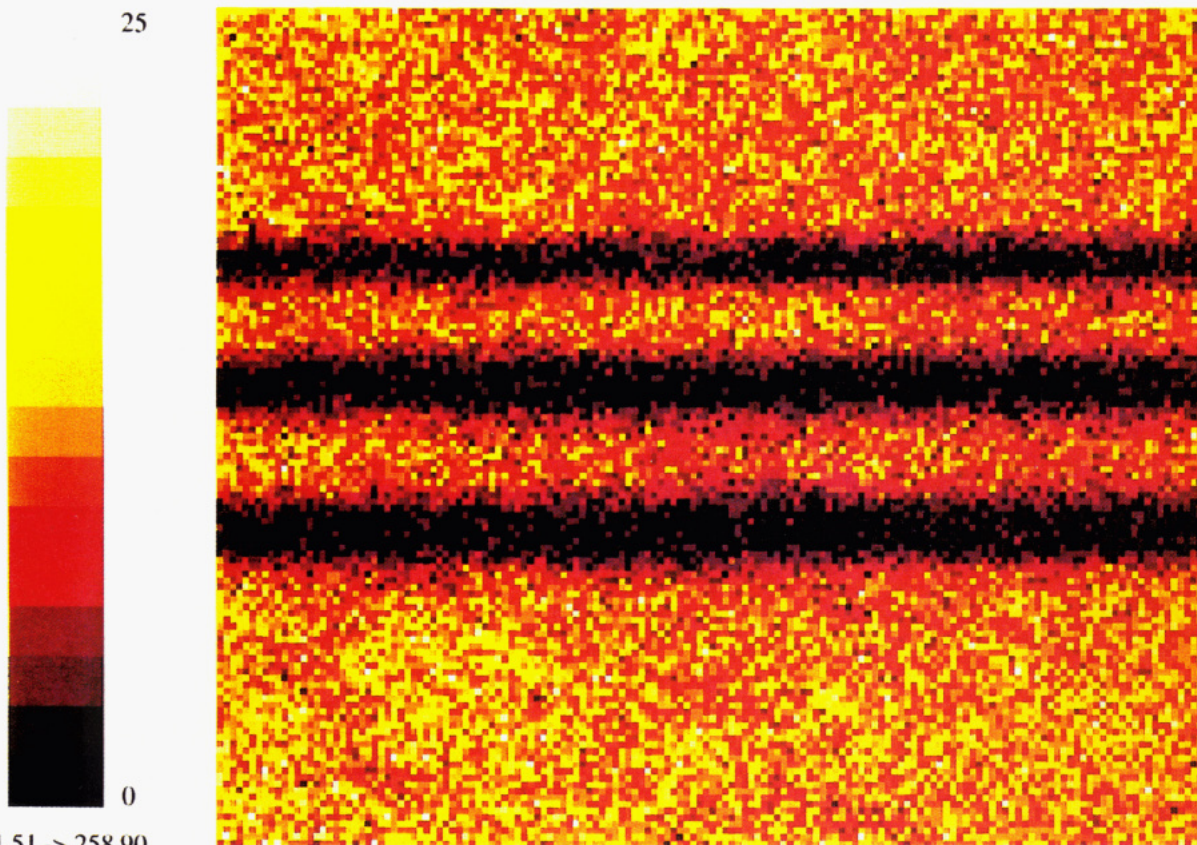


Figure 7. A $20 \mu\text{m} \times 17 \mu\text{m}$ view of a patterned benzo[*a*]pyrene-covered Cu surface. The lines were created by etching the target with 1×10^{15} , 3×10^{15} , and 8×10^{15} Ga^+ ions/ cm^2 , from top to bottom, respectively. The image contains 152×128 pixels and required 30 min to acquire.

dependent on target temperature. As seen in Figure 6, there is nearly a 1 order of magnitude decrease in signal for each 10 K drop in temperature, and the behavior closely resembles the predicted behavior shown in Figure 5. By 210 K, the gas-phase signal is negligible.

It is possible to crudely estimate the ionization efficiency of benzo[*a*]pyrene under these circumstances. At 310 K, we expect at equilibrium 1.3×10^6 molecules/ mm^3 , but count effectively 2730 ions. Assuming the extraction efficiency is $\sim 50\%$ and the analyzer transmission is $\sim 50\%$, these numbers suggest that $\sim 1\%$ of the molecules are being ionized without fragmentation. Because of the assumptions involving equilibrium, however, there could be a 1 order of magnitude error in this estimate.

At cryogenic temperatures, it is feasible to acquire spatially resolved spectra using the same procedure outlined for obtaining atomic maps. An example using benzo[*a*]pyrene is shown in Figure 7. For this image, a thin film of benzo[*a*]pyrene was deposited onto a clean Cu substrate. The precise thickness of the film is unknown, but enough material was deposited to form two or three molecular layers. This substrate was then patterned at 80 K by irradiating the target with a relatively high dose of Ga^+ ions generated from the LMIG itself. The image was created at 80 K by windowing the group of ions between m/z 248 and 252 which are characteristic of the molecular ion of benzo[*a*]pyrene. The image was obtained by bombarding each pixel with three Ga^+ ion pulses of 300 ns in length, corresponding to a total of 330 Ga^+ ions/pixel. For the magnification shown, each pixel measures $130 \text{ nm} \times$

130 nm in area, so the total dose is $2 \times 10^{12} \text{ Ga}^+$ ions/ cm^2 . Note that the brightest pixel contain 25 counts. Although the sputter yield of benzo[*a*]pyrene molecules is unknown, molecular dynamics computer simulations on related aromatic molecules³⁰ suggest it is in the range of 1–10 molecules/ Ga^+ ion. Hence, the useful yield of benzo[*a*]pyrene molecules is in the range of 0.75–7.5%. For this case, then, the numbers are not dramatically worse than those reported for In atoms. Moreover, they are at least 2 orders of magnitude higher than those found from the SIMS spectrum of benzo[*a*]pyrene.⁶

The image itself exhibits interesting characteristics. Note that the width of the line drawn by the LMIG is dependent upon the ion dose. Moreover, the nominal width of the incident beam is less than 200 nm, even though the narrowest line is ~ 800 nm in width. This effect could have several origins including ion-induced diffusion effects or thermally induced evaporation around the edges of the collision cascade. The incident beam itself, however, is known to possess significant intensity in its wings, which exhibit an approximately Lorenzian character. These wings extend nearly $1 \mu\text{m}$ away from the central spot. At higher doses, these wings produce a sufficient number of incident ions to produce measurable surface damage. This latter effect is the most likely cause of our observation. An upper limit to the image resolution may be estimated from the edge definition of these lines. Our analysis suggests that the region between light and dark is two pixels or 260 nm.

(30) Garrison, B. J. *J. Am. Chem. Soc.* **1980**, *102*, 6553–6555.

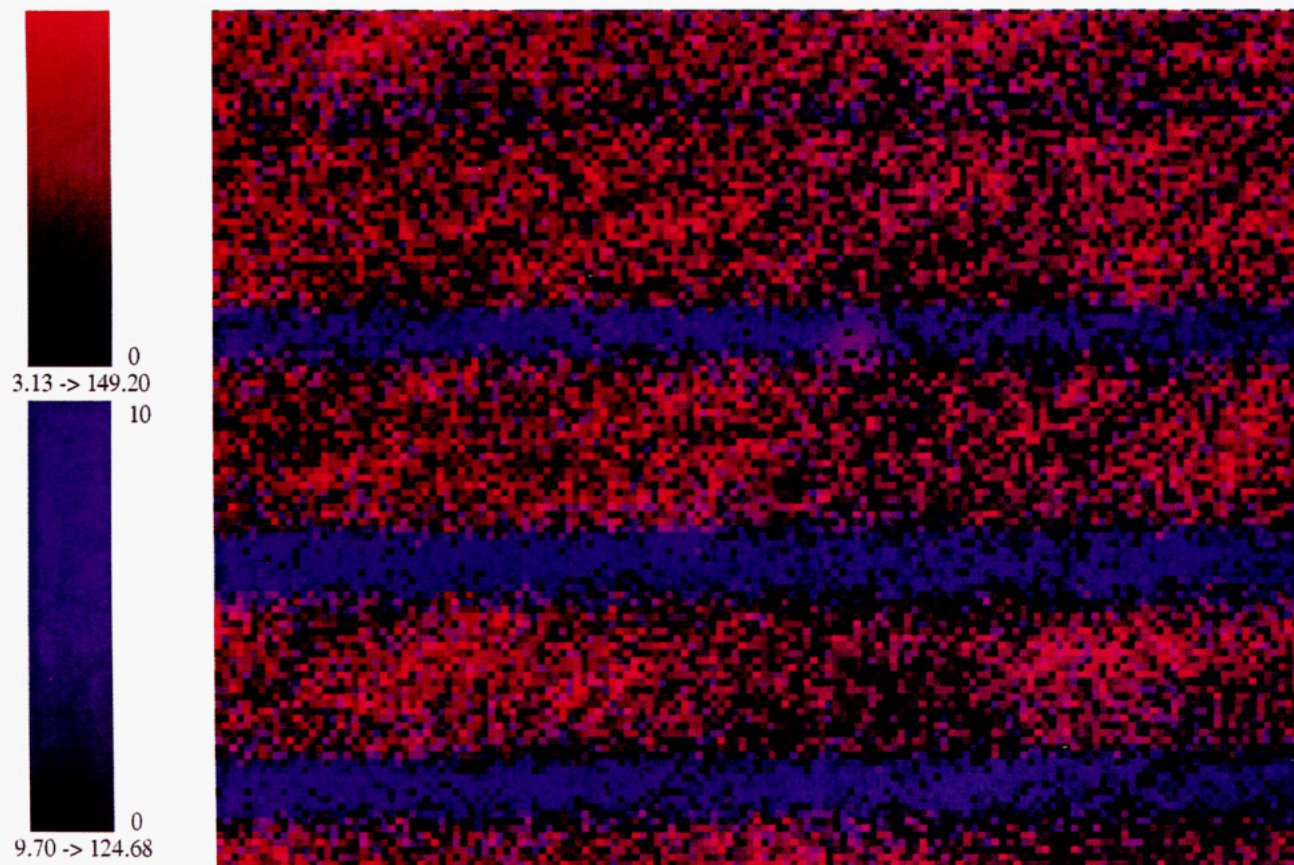


Figure 8. A $20 \mu\text{m} \times 17 \mu\text{m}$ view of a patterned tryptophan-covered surface. The lines were created by etching the target with 1×10^{15} , 2×10^{15} , and 4×10^{15} Ga^+ ions/ cm^2 , from top to bottom respectively. The very top line, which is only barely visible, was formed by etching with 3×10^{14} Ga^+ ions/ cm^2 . The red pixels represent the intensity of m/z 130, while the blue pixels represent m/z 107 and 109, the major isotopes of Ag. The image contains 152×128 pixels and required 50 min to acquire.

Many other molecular species are not as easy to ionize as benzo[*a*]pyrene, and it remains to be seen how valuable this approach will be for studying a wide range of molecules. We have examined other aromatic systems and found that the ionization efficiency is up to 1 order of magnitude lower than for benzo[*a*]pyrene when optimal laser conditions are found. For example, we show in Figure 8 an image recorded at 80 K of a film of tryptophan deposited on a silver substrate and etched in a manner identical to that followed for benzo[*a*]pyrene. This species does not produce a significant yield of molecular ions at m/z 204, but it is feasible to monitor a major fragment ion at m/z 130 corresponding to loss of $(\text{NH}_2)\text{CHCO}_2\text{H}$.^{19,23} To achieve necessary contrast, this image required five laser shots per pixel and yields three to five counts per laser shot. It should be noted that the spectrum obtained for positionized tryptophan is very similar to that obtained using UV 500-fs laser pulses, although the ionization efficiency in those experiments appears to be ~ 1 order of magnitude higher.¹⁹ The spatial resolution in our image is again on the order of 260 nm as determined by the sharpness of the line pattern. It was also possible to detect a sufficient intensity of nonresonantly ionized Ag atoms to obtain a Ag image which corresponds to the tryptophan image seen in Figure 8. These results are interesting since they show that the ion beam etching procedure used in forming the patterned layer actually removes tryptophan from the surface exposing Ag, rather than simply leaving a damaged layer of tryptophan molecules.

Our results at this stage certainly suggest that submicrometer molecular imaging is feasible using this approach. Moreover, due to the very low incident current achievable from LMIGs with submicrometer beam sizes and due to the vapor pressure of most molecular species, sample cooling is critical to achieving meaningful images free of background interferences. In general, we find that the cryogenic sampling procedure reported in this work performs smoothly and without adding undue complication to the analysis. It is necessary, however, to be careful to keep the operating pressure of the system in the 10^{-9} – 10^{-10} Torr range to prevent significant redeposition of gas-phase components onto the surface of interest. In Figure 9, for example, we show the SIMS spectrum of a Cu substrate cooled to 80 K and held for an extended period in a vacuum with a residual pressure of 1×10^{-7} Torr. Note the presence of a characteristic pattern of $\text{Cu}(\text{H}_2\text{O})_n\text{-Cu}(\text{H}_2\text{O})^+_n$ clusters, indicating that extensive deposition of H_2O has occurred on the initially clean Cu target. This redeposition may cover the molecules of interest, effectively reducing their sputtering yield.

CONCLUSIONS AND PROSPECTS

In this work, we have examined several issues that are important for achieving molecule-specific mapping with submicrometer spatial resolution. The overriding limitation of these experiments is, of course, the decreasing number of surface molecules available for detection as the size of the ion

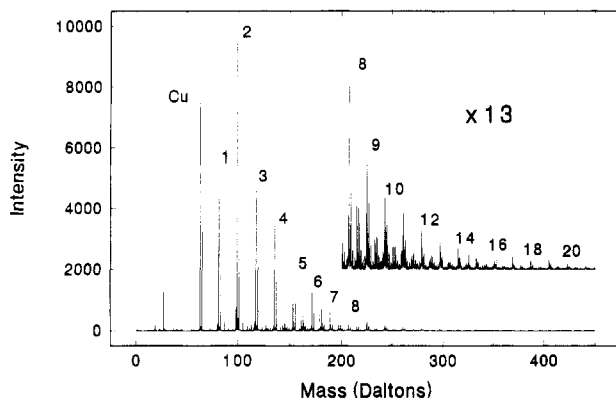


Figure 9. TOF-SIMS spectrum of a Cu sample held at 80 K in a residual vacuum of 1×10^{-7} Torr for 30 min. Although the Cu signal is certainly very strong, $\text{Cu}(\text{H}_2\text{O})_n^+$ clusters, with $n = 1-20$, are clearly visible.

beam probe is reduced to this spatial regime. Our proposal, and that of others,¹³⁻¹⁹ is to employ laser postionization to increase the sensitivity over that obtainable with SIMS.

Several factors have been identified here which make the goal of chemical mapping quite challenging. The current in the primary beam probe is very low, making the sputtered flux often much smaller than the vapor pressure of the molecular target under study. Moreover, the low repetition rate of the pulsed laser source means that image acquisition time will be quite long—on the order of 30–60 min in favorable cases. And finally, although multiphoton ionization may produce molecular ions with yields up to 1%, these yields are often significantly lower and are complicated by photofragmentation processes. Even though it may be possible in some cases to exceed the static limits,¹² achievement of the best possible images requires essentially 100% molecular photoionization.

On the positive side, we have shown that, for atomic species, very high useful yields may be achieved, along with images with spatial resolution in the 100-nm range. For molecular species, the vapor pressure background problem may be solved by simply cooling the target. In favorable cases, molecular maps may be obtained with 260-nm spatial resolution, well below our submicrometer goal. Ionization efficiencies are generally higher than those found for SIMS alone, although further improvements in this area are clearly necessary.

There are presently a number of developments in laser technology which promise to dramatically enhance the value of postionization methods, particularly for imaging. The initial results using subpicosecond pulses look quite promising for achieving higher ionization efficiencies for molecules. Moreover, the latest Ti:Sapphire lasers are capable of producing $>100 \mu\text{J}$ of UV light with pulse repetition rates of 1–5 kHz and pulse widths of <200 fs. Incorporation of these advances into the ion microprobe could speed the image acquisition time by 2 orders of magnitude and improve the sensitivity by 1 or 2 orders of magnitude.

ACKNOWLEDGMENT

The authors thank Steve Mullock and Clive Corlett of Kore Technology for their design of the cryogenic sample stage. Partial financial support from the Department of Energy, the National Institutes of Health, the Office of Naval Research, and the National Science Foundation is greatly appreciated.

Received for review April 25, 1994. Accepted May 23, 1994.^a

^a Abstract published in *Advance ACS Abstracts*, June 15, 1994.